

Review

# Recent Progress of Toxic Gas Sensors Based on 3D Graphene Frameworks

Qichao Dong, Min Xiao, Zengyong Chu \*, Guochen Li and Ye Zhang

College of Liberal Arts and Science, National University of Defense Technology, Changsha 410073, China; qichao\_dong@163.com (Q.D.); a2805173694@163.com (M.X.); lgc\_nudt@126.com (G.L.); zhangye8905@foxmail.com (Y.Z.)

\* Correspondence: chuzy@nudt.edu.cn

**Abstract:** Air pollution is becoming an increasingly important global issue. Toxic gases such as ammonia, nitrogen dioxide, and volatile organic compounds (VOCs) like phenol are very common air pollutants. To date, various sensing methods have been proposed to detect these toxic gases. Researchers are trying their best to build sensors with the lowest detection limit, the highest sensitivity, and the best selectivity. As a 2D material, graphene is very sensitive to many gases and so can be used for gas sensors. Recent studies have shown that graphene with a 3D structure can increase the gas sensitivity of the sensors. The limit of detection (LOD) of the sensors can be upgraded from ppm level to several ppb level. In this review, the recent progress of the gas sensors based on 3D graphene frameworks in the detection of harmful gases is summarized and discussed.

**Keywords:** graphene; graphene hydrogel; graphene aerogel; gas sensor



**Citation:** Dong, Q.; Xiao, M.; Chu, Z.; Li, G.; Zhang, Y. Recent Progress of Toxic Gas Sensors Based on 3D Graphene Frameworks. *Sensors* **2021**, *21*, 3386. <https://doi.org/10.3390/s21103386>

Academic Editor: Paolo Bertoncello

Received: 7 April 2021

Accepted: 8 May 2021

Published: 13 May 2021

**Publisher's Note:** MDPI stays neutral with regard to jurisdictional claims in published maps and institutional affiliations.



**Copyright:** © 2021 by the authors. Licensee MDPI, Basel, Switzerland. This article is an open access article distributed under the terms and conditions of the Creative Commons Attribution (CC BY) license (<https://creativecommons.org/licenses/by/4.0/>).

## 1. Introduction

There is a huge demand for the development of simple and reliable gas sensors [1]. In many fields, such as agriculture, medical diagnosis, and industrial waste, especially in environmental monitoring, it is necessary to detect NO<sub>x</sub> (especially NO<sub>2</sub>), ammonia (NH<sub>3</sub>), and volatile organic compounds (VOCs), because of their possible toxicity and related risks to the ecosystem [2,3]. In many countries, air pollution is a major environmental problem caused by rapid industrialization. A large amount of NO<sub>2</sub> is emitted into the environment every year due to the industrial combustions and automobile emissions [4]. Therefore, the detection of NO<sub>2</sub> has aroused widespread concerns, because it is harmful to the plants and respiratory systems of people and animals [5]. Additionally, NO<sub>2</sub> can cause acid rain and photochemical smog [6,7]. Therefore, the United States Environmental Protection Agency (EPA) defines NO<sub>2</sub> as a typical air pollutant, and the exposure limit is only 53 ppb [8]. Ammonia (NH<sub>3</sub>) is also a common dangerous air pollutant, which is produced by the industrial process, agricultural production, and manufacturing process [9,10]. Specifically, any overexposure to the high concentrations of NH<sub>3</sub> (>30 ppm, 10 min) can irritate the human eye, skin, and respiratory system [11–13]. VOCs are the hydrocarbons that exist as gases or vapor at room temperature, which can be emitted from numerous products and activities, e.g., detergents, paints, solvents, tools, clothes, toys, cleaning, and cooking [14]. Aldehyde, aromatic, aliphatic, halogenated, and terpenoid compounds are the VOCs commonly detected in commercial buildings [14,15]. Toxic VOCs that have been previously detected in air by any type of sensors include formaldehyde, acetaldehyde, benzene, toluene, xylenes, phenol, pyridine, acetone, acetic anhydride, carbon disulfide, dihydroxybenzene, and so on [14–19]. For example, phenol is a toxic VOC occurring both naturally but also from industrial processes, which can be rapidly absorbed through the skin and cause skin and eye burns upon contact [20]. It is considered as a serious pollutant because of the toxicity and persistence in the environment. The short-term exposure limit of phenol is 10 ppm, 60 min [21]. Because of the serious environmental pollution, phenol

monitoring becomes an urgent problem. Therefore, with the monitoring development of air pollution, the demand for gas sensors will increase rapidly in the future.

As a 2D material, graphene has many advantages, such as large conjugated structure, high specific surface area, high conductivity, easy to be synthesized, sensitive to the gas molecules, and so on. It has been proven to be a promising high-performance gas detection material [22]. Graphene surface can easily absorb some molecules, such as NO<sub>2</sub>, NH<sub>3</sub>, CO<sub>2</sub>, and so on. Moreover, the conductivity of graphene will change after adsorption of target gas molecules. The concentration of target gas in the environment can be detected by monitoring the change of conductivity. There have been many reports on the application of graphene in gas sensors, including pure graphene [23–26] and graphene composite materials [27–31]. There are many factors affecting graphene-based sensors, including: synthetic method [32–34], chemical structure [35–37], interlaminar structure [34,38], testing environment [39–42], and surface properties [43–47]. Due to the  $\pi$ - $\pi$  accumulation and Van Der Waals force binding between graphene, the 2D graphene nanocomposites tend to agglomerate, resulting in the reduction of specific surface area [48–50]. In order to make full use of the characteristics of graphene, 2D graphene is usually assembled into a three-dimensional (3D) framework state by a series of methods. In contrast, due to the combination of 3D porous structure and the inherent characteristics of graphene, 3D graphene provides more space and larger surface area to transport and store electrons. 3D graphene has good conductivity, large specific surface area, and versatile gas adsorption sites. Furthermore, the defects and edge positions on the 3D porous graphene play an important role in promoting gas adsorption [48]. In recent years, compared with 2D graphene structures, 3D porous graphene structures such as graphene hydrogels, graphene aerogels, and graphene foams have been used as high-performance gas sensors [49]. Although 3D graphene has broad prospects in the field of gas sensors with the super high sensitivity, the selectivity is not satisfactory. Different gas molecules may adsorb on the same 3D graphene sheets and lead to the total change of the resistance [50,51]. It is difficult to quantitatively distinguish one target gas from a gas mixture. To improve the selectivity, defect engineering is generally needed to modulate graphene [52].

Several reviews have presented the main development of graphene-based gas sensors. For example, in 2015, Meng et al. [49] reviewed the graphene-based hybrids for chemiresistive gas sensors. They focused on the sensing principles and synthesis processes of the graphene-based hybrids with noble metals, metal oxides, and conducting polymers. In 2018, Xia et al. [50] summarized the 3D structure graphene/metal oxide hybrids for gas sensors. They concluded a variety of logical strategies to design the 3D nanohybrids of RGO and MOx. In 2020, Ilnicka et al. [51] summarized the graphene-based hydrogen gas sensors, a special case of gas sensitivity to H<sub>2</sub>. However, the above reviews did not reflect the whole progress of graphene gas sensors, especially for the air pollution monitoring applications. This paper aims to summarize the recent progress of the gas sensors based on 3D graphene frameworks in the detection of air pollutants.

## 2. Synthesis of 3D Graphene Frameworks

Graphene oxide (GO) and reduced graphene oxide (RGO) have a 2D conjugated structure with single-atom thickness and residual oxygen-containing groups, which can be regarded as 2D conjugated macromolecules, structurally. They have rich chemical activities, which are helpful for 3D self-assembly through a series of chemical modification methods to regulate the interaction between the layers [34,38].

Graphene hydrogel is one of the major 3D assemblies. Chemically modified graphene (CMG) hydrogels prepared from GO or RGO can be used for large-scale production. As shown in Figure 1, RGO hydrogels (RGOHs) can be obtained by the following methods:

- (1) Hydrothermal reduction, which is simple, fast, and free of impurities. At present, the commonly used hydrothermal method is to prepare RGO dispersion by hydrothermal treatment at 180 °C [53–55].

- (2) Chemical reduction, which is beneficial for large-scale production, and various reducing agents can be selected [56–65].
- (3) Electrochemical reduction [66–68]. The hydrogel prepared by this method is applied to the electrode surface and can be directly applied to the electrode materials of electrochemical instruments.
- (4) Vacuum filtration. A simple vacuum filtration method was developed to prepare RGO hydrogels with high conductivity, anisotropy, and responsive stimuli [69,70].

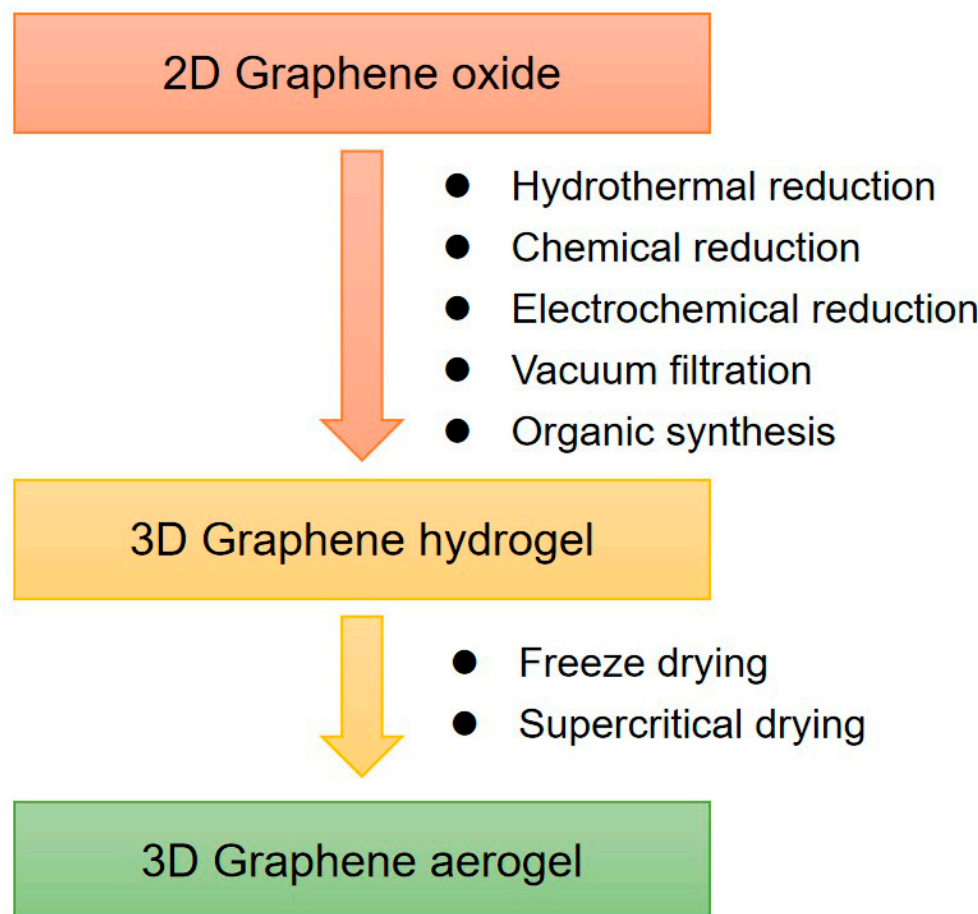


**Figure 1.** Synthesis methods of 3D graphene frameworks.

In addition to the 3D self-assembly of graphene in a water system, the assembly of the graphene in an organic system can also be achieved by thermal solvent reduction [71–73].

Graphene aerogel composites are usually prepared by supercritical drying or freeze-drying of hydrogel precursors [74,75]. For example, highly compressible RGO aerogels can be obtained by freeze-drying and microwave treatment. Directional freezing is a well-known processing technology of porous materials. This technology can also be used for the preparation of graphene aerogels [76]. Moreover, the controllable heat treatment technology can also reduce GO to RGO and restore conductivity. The regulation of the chemical structure of GO can adjust the morphology and elasticity of aerogels, for example, the oxygen functional groups in GO have a significant effect on the morphology and elasticity of the gels [77].

### 3. NO<sub>2</sub> Gas Sensors

The development of a highly selective NO<sub>2</sub> gas sensor with ppb detection limit is an important requirement for continuous environmental monitoring [78] and early diagnosis of respiratory diseases [79]. However, the original graphene, RGO, and RGOH had limited

reaction to  $\text{NO}_2$ , and could not monitor  $\text{NO}_2$  gas below 100 ppb [80]. Therefore, researchers have explored a variety of methods to fabricate graphene composites. Compared with 2D RGO, 3D RGO is more sensitive to  $\text{NO}_2$  [81]. Table 1 lists the gas sensitivities of 3D graphene toward  $\text{NO}_2$ . The response is generally given in the form of relative change of resistance ( $\Delta R/R_0$ ) or conductance ( $\Delta G/G_0$ ), which was tested at a set temperature and a set concentration of  $\text{NO}_2$ .  $S_{3D}$  and  $S_{2D}$  are the sensitivities (responses per ppm) of 3D and 2D graphene, respectively. The graphene with a 3D structure can increase the gas sensitivity to one or two orders of magnitude higher. The LOD of the sensors can be upgraded from ppm level to several ppb level.

**Table 1.** Gas sensitivities of 3D graphene toward  $\text{NO}_2$ .

3D Graphene	Temp. (°C)	$C_{\text{NO}_2}$ (ppm)	Response	$S_{3D}$ (ppm $^{-1}$ )	$S_{3D}/S_{2D}$	Recovery Time (s)	LOD (ppb)	Year	Ref.
Superhydrophobic 3D RGO	113	1	$\Delta G/G_0 = 23.5\%$	23.5%	-	169	9.1	2018	[82]
3D S-RGOH	RT	2	$\Delta R/R_0 = 22.5\%$	8.7%	118.6	11	4.1	2017	[83]
3D RGO-SnO <sub>2</sub>	55	100	$\Delta R/R_0 = 6.5\%$	0.1%	-	500	2000	2015	[84]
3D SnO <sub>2</sub> /RGOH	RT	5	$\Delta G/G_0 = 32\%$	4.3%	62.9	260	2.8	2020	[85]
3D MoS <sub>2</sub> /RGO	80	10	$\Delta I/I_0 = 2483\%$	248%	>250	30	27.9	2019	[52]
3D SnS <sub>2</sub> /RGO	RT	8	$\Delta G/G_0 = 49.8\%$	6.1%	22.6	76	8.7	2020	[86]
3D N-RGOH	RT	0.8	$\Delta G/G_0 = 11.7\%$	8.7%	18	10	14	2019	[87]
3D B-RGOH	RT	0.8	$\Delta G/G_0 = 25.3\%$	20%	38.9	90	9	2019	[87]
3D RGO/Eu(TPyP) (Pc)	RT	20	$\Delta I/I_0 = 12\%$	0.6%	2	828	80	2020	[88]
VC-Funct. RGOH	RT	10	$\Delta G/G_0 = 36.3\%$	3.6%	10	300	100	2020	[89]

Note: The response, in the form of relative change of resistance ( $\Delta R/R_0$ ) or conductance ( $\Delta G/G_0$ ), was tested at a set temperature and a set concentration of  $\text{NO}_2$  ( $C_{\text{NO}_2}$ ).  $S_{3D}$  and  $S_{2D}$  are the sensitivities (responses per ppm) of 3D and 2D graphene, respectively. LOD = limit of detection.

### 3.1. 3D MoS<sub>2</sub>/RGO

2D-layered MoS<sub>2</sub> is an excellent gas sensing material due to its high surface/volume ratio and excellent electronic properties [90–94]. However, MoS<sub>2</sub> nanoparticles tend to agglomerate, which limits their applications. Loading MoS<sub>2</sub> on 3D RGO is a good choice [95–97]. Chen et al. [52] reported a highly sensitive  $\text{NO}_2$  sensor based on 3D MoS<sub>2</sub>/RGO composites. The composites were prepared using a novel self-assembly and hydrothermal method. The mild synthesis process enables MoS<sub>2</sub> to uniformly disperse on the 3D RGO framework. The agglomeration of MoS<sub>2</sub> was significantly alleviated, resulting in excellent low-temperature sensing performance. Figure 2 shows the fabrication process, gas responses, and sensing mechanism of the 3D MoS<sub>2</sub>/RGO sensor. The selectivity of the fabricated sensors was characterized using a variety of independent gases. The device shows higher sensing response towards N-based molecules (e.g.,  $\text{NO}_2$ ,  $\text{NH}_3$ ) than the other gases (CO,  $\text{C}_2\text{H}_5\text{OH}$ ,  $\text{H}_2$ , HCHO). When the sensor is exposed to  $\text{NO}_2$  atmosphere, the minority charge carriers (electrons) in the MoS<sub>2</sub>/rGO composites will transfer to  $\text{NO}_2$  due to the strong electron negativity of  $\text{NO}_2$ . Thus, the width and height of the heterojunction are reduced, leading to the increased conductivity. A small variation in barrier height and width caused by gas adsorption or desorption can have a significant influence on the resistance. A superior low-temperature  $\text{NO}_2$  sensing performance with a response of 2483% toward 10 ppm  $\text{NO}_2$  was achieved at 80 °C.

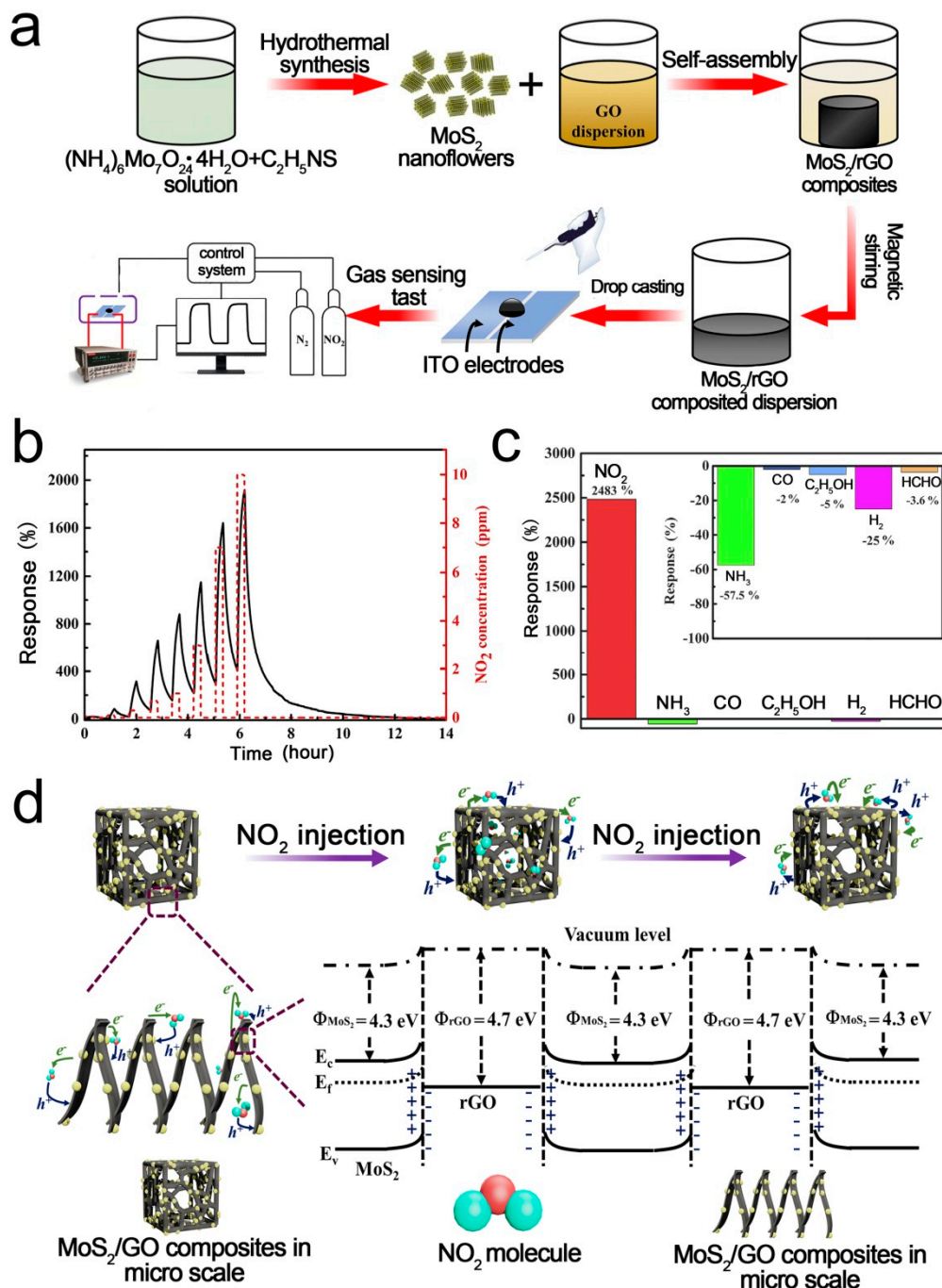


**Figure 2.** (a) Fabrication process of 3D MoS<sub>2</sub>/RGO; (b) Dynamic gas responses of MoS<sub>2</sub>/RGO; (c) Responses of MoS<sub>2</sub>/RGO-5; (d) Schematic illustration of the sensing mechanism [52].

### 3.2. 3D SnS<sub>2</sub>/RGO

Different from *p*-type RGO, SnS<sub>2</sub> is an *n*-type semiconductor with an indirect band gap of 2.2 eV [98]. SnS<sub>2</sub> has a high affinity to NO<sub>2</sub> because of its much weaker electronegativity than NO<sub>2</sub> [99,100]. However, the resistance of SnS<sub>2</sub> is too high to be measured at room temperature, so SnS<sub>2</sub> is not suitable for monitoring NO<sub>2</sub> at room temperature. When SnS<sub>2</sub> is coupled with 3D graphene, their properties are complementary to each other. Wu et al. [86] demonstrated a kind of 3D structured SnS<sub>2</sub>/RGO heterojunction, which was synthesized through a facile hydrothermal route. Figure 3 shows the microstructure, gas responses, and sensing mechanism of the SnS<sub>2</sub>/RGO sensor. The 3D structure enhances the adsorption and

diffusion of small  $\text{NO}_2$  molecules.  $\text{SnS}_2$  can facilitate the electron transfer from RGO to  $\text{NO}_2$  by forming a heterojunction with RGO. The depletion layer with an electrostatic field at the *p-n* heterojunction region could promote the dissociation of  $\text{NO}_2$  and thus enhance the  $\text{NO}_2$  adsorption at low temperatures. Upon  $\text{NO}_2$  adsorption on  $\text{SnS}_2$ , the electron will transfer from  $\text{SnS}_2$  to  $\text{NO}_2$ , leading to the increase both of the electron-depletion region and the hole concentration of the *p*-type RGO. Thus, the resistance of  $\text{SnS}_2/\text{RGO}$  is reduced. The sensor displays impressive  $\text{NO}_2$  sensing performance, including high sensitivity ( $6.1 \text{ ppm}^{-1}$ ), low LOD (8.7 ppb), good linearity, and reversibility.

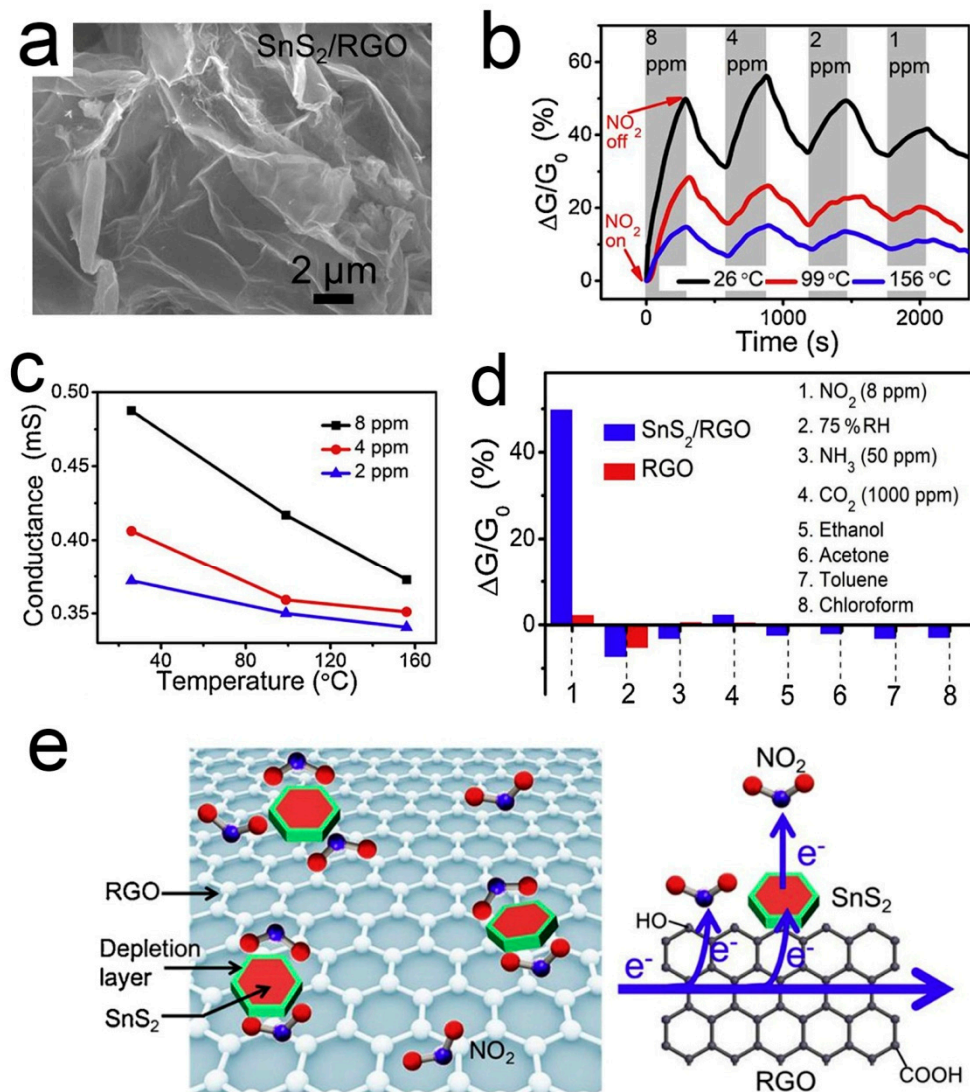


**Figure 3.** (a) SEM image of 3D  $\text{SnS}_2/\text{RGO}$ ; (b) Dynamic responses of  $\text{SnS}_2/\text{RGO}$  to  $\text{NO}_2$ ; (c) Conductance variation of  $\text{SnS}_2/\text{RGO}$  versus operation temperature; (d) RT sensing responses of  $\text{SnS}_2/\text{RGO}$  and RGO; (e) Schematic illustration of the  $\text{NO}_2$  sensing mechanism of the  $\text{SnS}_2/\text{RGO}$  sensor [86].

### 3.3. 3D Eu(TPyP)(Pc)/RGO

Pure RGO sensors have poor selectivity, slow response, and long recovery time, which limits their wide applications [89]. Chemical/physical modification with the external groups or atoms is an effective method [101,102]. Zhu et al. [88] reported a sandwich-type double-decker complex Eu(TPyP)(Pc) (TPyP = meso-tetra(4-pyridyl)porphyrin; Pc = phthalocyanine), which was in situ self-assembled on the surface of RGO driven by the  $\pi-\pi$  interaction, forming a 3D RGO/Eu(TPyP)(Pc) hybrid aerogel. Eu(TPyP)(Pc) not only acts as a sensor recognition unit, but also helps to enhance the amplification effect of the *p-n* heterojunc-

tion. At the same time, it provides enough space for the efficient transmission of RGO. The resulting aerogel not only effectively integrates the gas sensing of Eu(TPyP)(Pc) and good conductivity of RGO, but also exhibits a prominent synergy effect. Figure 4 shows the microstructure, responses, and working mechanism of the RGO/Eu(TPyP)(Pc) sensor. A good linear ratio between signal response and target gas concentration is achieved in the range of 0.5–20 and 20–100 ppm.

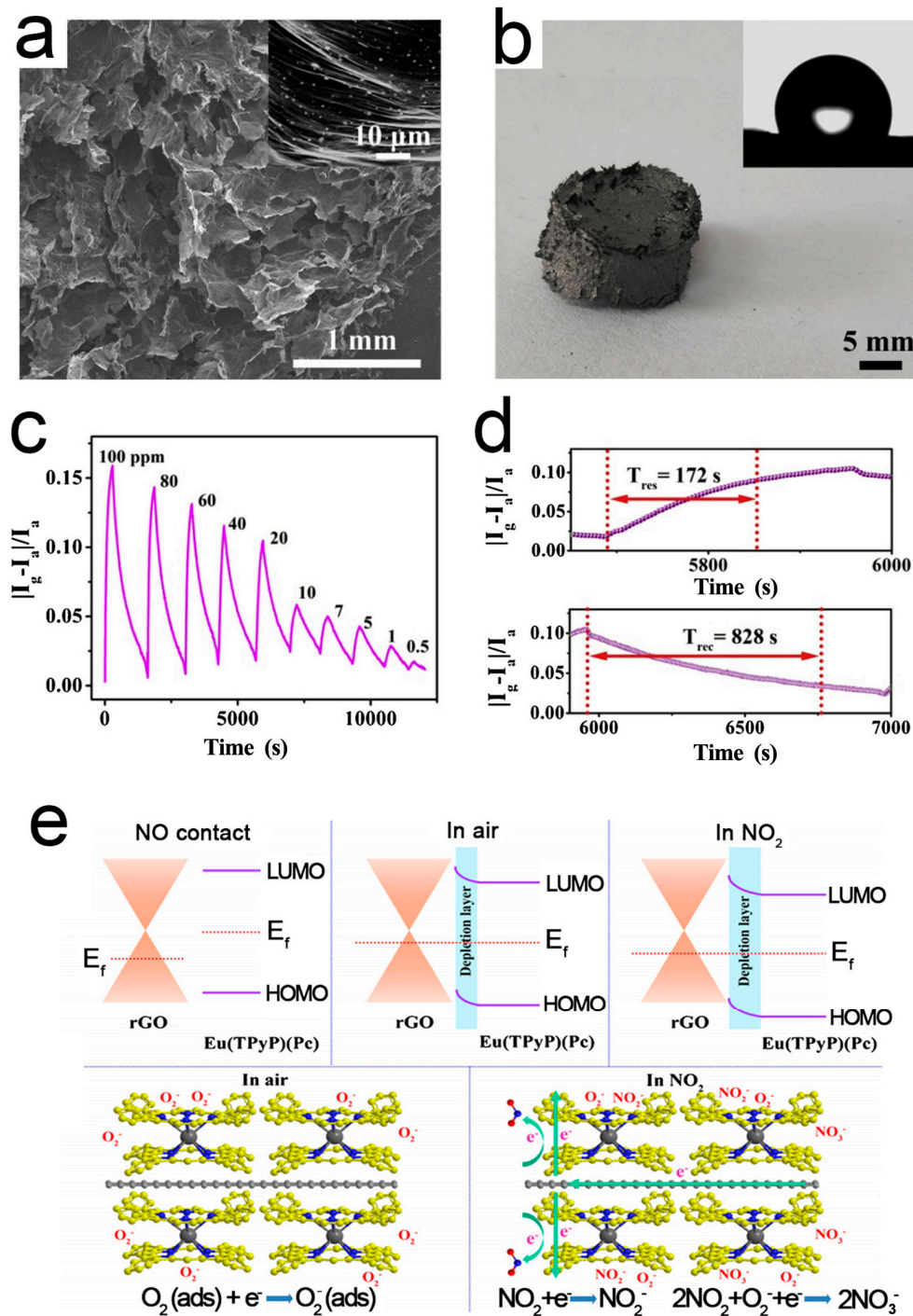


**Figure 4.** (a) SEM image of RGO/Eu(TPyP)(Pc); (b) Photograph of RGO/Eu(TPyP)(Pc); inset: water contact angle. (c) Dynamic responses of RGO/Eu(TPyP)(Pc) to NO<sub>2</sub>; (d) Response-recovery time of RGO/Eu(TPyP)(Pc) to 20 ppm NO<sub>2</sub>; (e) Working mechanism of the RGO/Eu(TPyP)(Pc) sensor [88].

### 3.4. 3D $\text{SnO}_2/\text{RGOH}$

Many studies have been devoted to improving the gas sensitivity by immobilizing  $\text{SnO}_2$  crystals on RGO [103,104]. Li and co-workers used  $\text{SnO}_2$  nanocrystals supported by the 3D mesoporous graphene aerogels to detect  $\text{NO}_2$  gas at low temperature [84]. Wu et al. [85] reported a facile preparation of  $\text{SnO}_2$ -modified graphene hydrogel ( $\text{SnO}_2/\text{RGOH}$ ) via the one-step hydrothermal method. 3D  $\text{SnO}_2/\text{RGOH}$  was synthesized directly from  $\text{Sn}^{2+}$  and GO precursors without any surfactant. The results show that it is feasible to optimize the gas sensing performance by combining reasonable material hybridization, 3D structure, and temperature modulation. The  $\text{SnO}_2/\text{RGO}$  hybrid showed a high sensitivity to  $\text{NO}_2$  [105]. The improved sensitivity is due to the agglomeration of  $\text{SnO}_2$  nanoparticles and the formation of *p-n* heterojunction at the interface between  $\text{SnO}_2$  and RGO [106]. The *p-n* heterojunction formed at the interface of RGOH and  $\text{SnO}_2$  promotes the charge transfer. A micro-heater is integrated on the other side of the substrate to increase the substrate temperature locally, so as to suppress the interference of humidity in  $\text{NO}_2$  sensing. Figure 5 shows the microstructure, gas responses, and selectivity of the flexible  $\text{SnO}_2/\text{RGOH}$  sensor. When exposed to 0.5–5 ppm  $\text{NO}_2$ ,  $\text{SnO}_2/\text{RGOH}$  showed an immediately increased conductivity.

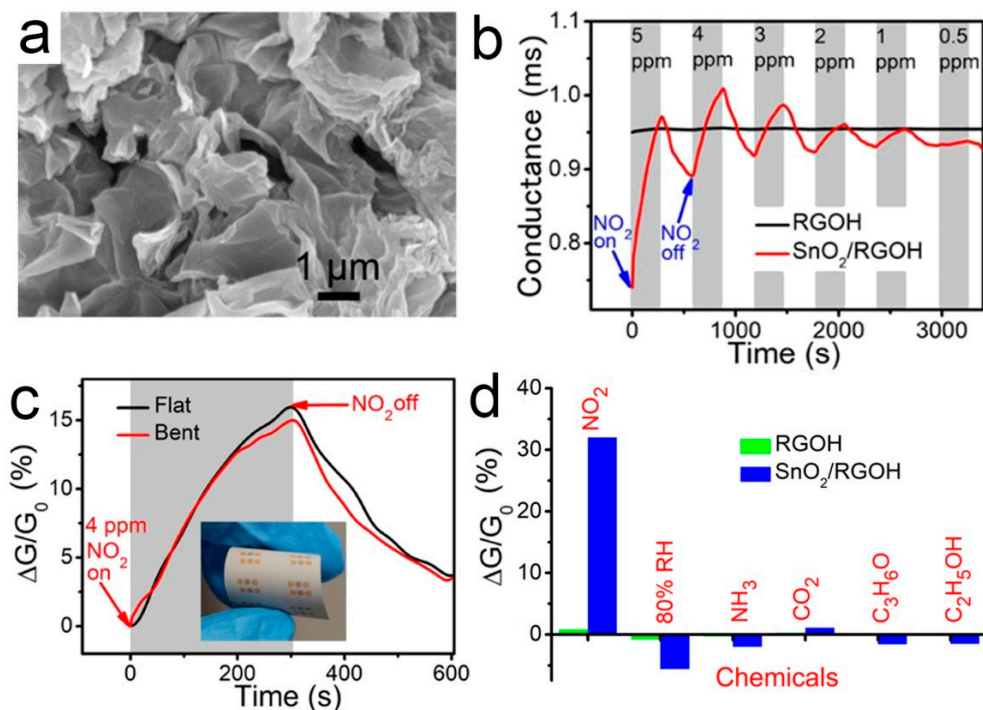


**Figure 5.** (a) SEM image of 3D  $\text{SnO}_2/\text{RGOH}$ ; (b) Dynamic responses of RGOH and  $\text{SnO}_2/\text{RGOH}$  to  $\text{NO}_2$ ; (c) RT responses of  $\text{SnO}_2/\text{RGOH}$  and RGOH; (d) Real-time responses of the flexible  $\text{SnO}_2/\text{RGOH}$  sensor. Inset: Photograph of the sensor with the bent angle of 150° [85].

### 3.5. 3D Porous B- and N-Doped RGOH

Recent studies have shown that doping is a feasible strategy to adjust the physical, electronic, and chemical properties of graphene by creating a band gap [107]. Under the stable adsorption configuration, different elements in graphene can exhibit different gas sensing behaviors due to the different adsorption energy and the distance between doped atoms and gas molecules [108–110]. B- and N-doping can improve the selectivity of the graphene-based  $\text{NO}_2$  sensor [111–114]. Wu et al. [87] reported a 3D porous B- and N-doped RGOH chemical resistor. B- and N-RGOH were synthesized using a hydrothermal self-assembly method with the aid of boric acid ( $\text{H}_3\text{BO}_3$ ) and dicyandiamide ( $\text{C}_2\text{H}_4\text{N}_4$ ). Figure 6 shows the fabrication process, microstructures, and gas responses of the sensors. It shows that the combination of 3D hierarchical structure and the doping of B- and N-heteroatoms

can significantly improve the sensing performance. The response of B- and N-RGOH to  $\text{NO}_2$  is more than one order of magnitude higher than that of RGOH. It is worth noting that the response of B- and N-RGOH sensors varies almost linearly with the concentration of  $\text{NO}_2$ .

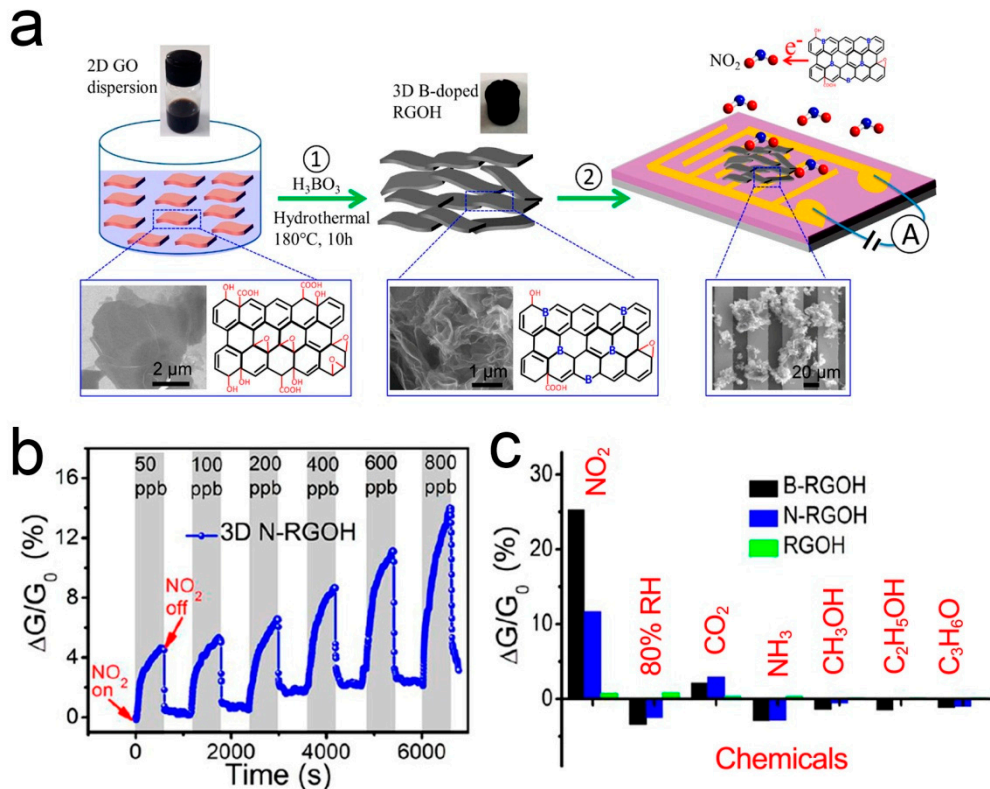


**Figure 6.** (a) Fabrication process of B-RGOH sensors. (b) Responses of B- and N-RGOH sensors to  $\text{NO}_2$ . (c) Responses of B- and N-RGOH sensors to different vapors [87].

#### 4. $\text{NH}_3$ Gas Sensors

The ammonia ( $\text{NH}_3$ ) sensor is indispensable in many industries and daily life. However, due to its complex preparation process, strict environmental requirements, and desorption of residual ammonia molecules, the production cost is high, which hinders the market acceptance [115–117]. The ammonia sensor might exhibit a reduced response during the recovery process in the co-presence of ammonia and ethanol, due to the result of multistep gas adsorption and desorption processes on material surface [115]. In general, the ammonia sensing behavior of the semi-conductive graphene-based sensors is negative to that of  $\text{NO}_2$  sensing, because  $\text{NH}_3$  is the reductive gas and  $\text{NO}_2$  is the oxidative gas [116,117]. For the same graphene-based sensors, however, the sensing performance toward  $\text{NH}_3$  is mostly reported as inferior to that toward  $\text{NO}_2$ , for example, in 2020, Wu et al. [89] reported a green synthesis method of 3D chemically functionalized graphene for the high-performance detection of  $\text{NH}_3$  and  $\text{NO}_2$  at room temperature. They found that the LOD of  $\text{NH}_3$  and  $\text{NO}_2$  were 500 and 100 ppb, respectively.

##### 4.1. 3D Graphene

Generally, when a sensor is recovered at room temperature, the gas molecules cannot be completely desorbed, resulting in poor stability and long recovery time [118]. The desorption of ammonia can be promoted using the infrared light source. This is attributed to the generation of charge carriers by absorbing infrared light [119]. Most of the others used heating to accelerate the desorption process, based on the principle of thermally excited gas molecules [120]. Wu et al. [121] used laser direct writing to fabricate three parallel porous 3D graphene lines on a polyimide (PI) tape to simply construct an ammonia

gas sensor. In this study, the ammonia sensor is located in the middle and the two sides are used as heaters. Voltage can be applied to the heater to promote desorption, as shown in Figure 7. The recovery time is relatively stable with the increase of the number of cycles, indicating that the residual ammonia molecules in the element are almost fully desorbed.

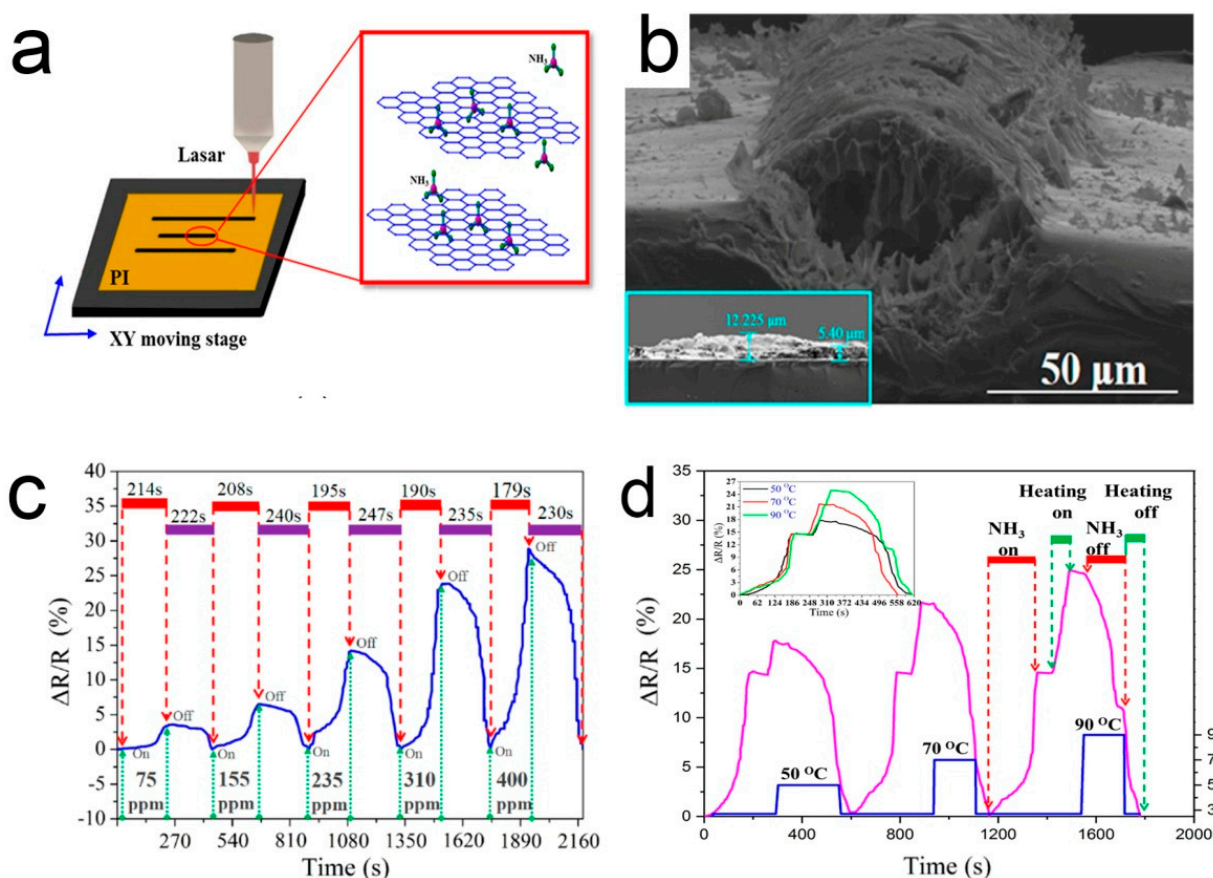


**Figure 7.** (a) A diagram of laser direct writing; (b) SEM side view image of the laser-irradiated PI; (c) The real-time response/recovery behaviors of the sensor; (d) The normalized real-time response/recovery behaviors of the sensor [121].

#### 4.2. 3D RGO/PPy

Recent studies have witnessed the significant progress of gas sensors based on polypyrrole (PPy) conducting polymers [122–125]. However, the serious agglomeration of the nanoparticles leads to a significant decrease in the visible active surface of gas molecules, which leads to the decrease of response sensitivity [126–128]. Qin et al. [129] used 3D RGO as a 3D skeleton support for the sensitive PPy nanoparticles. It has made an important contribution to improve the conductivity, dynamic performance, and sensing response, as shown in Figure 8. Highly dispersed and low agglomerated PPy nanoparticles are uniformly distributed on the pore walls of 3D RGO. The response to NH<sub>3</sub> can rapidly reach sub-ppm level, 4–5 times more sensitive than that of pure PPy. The sensor has perfect stability.

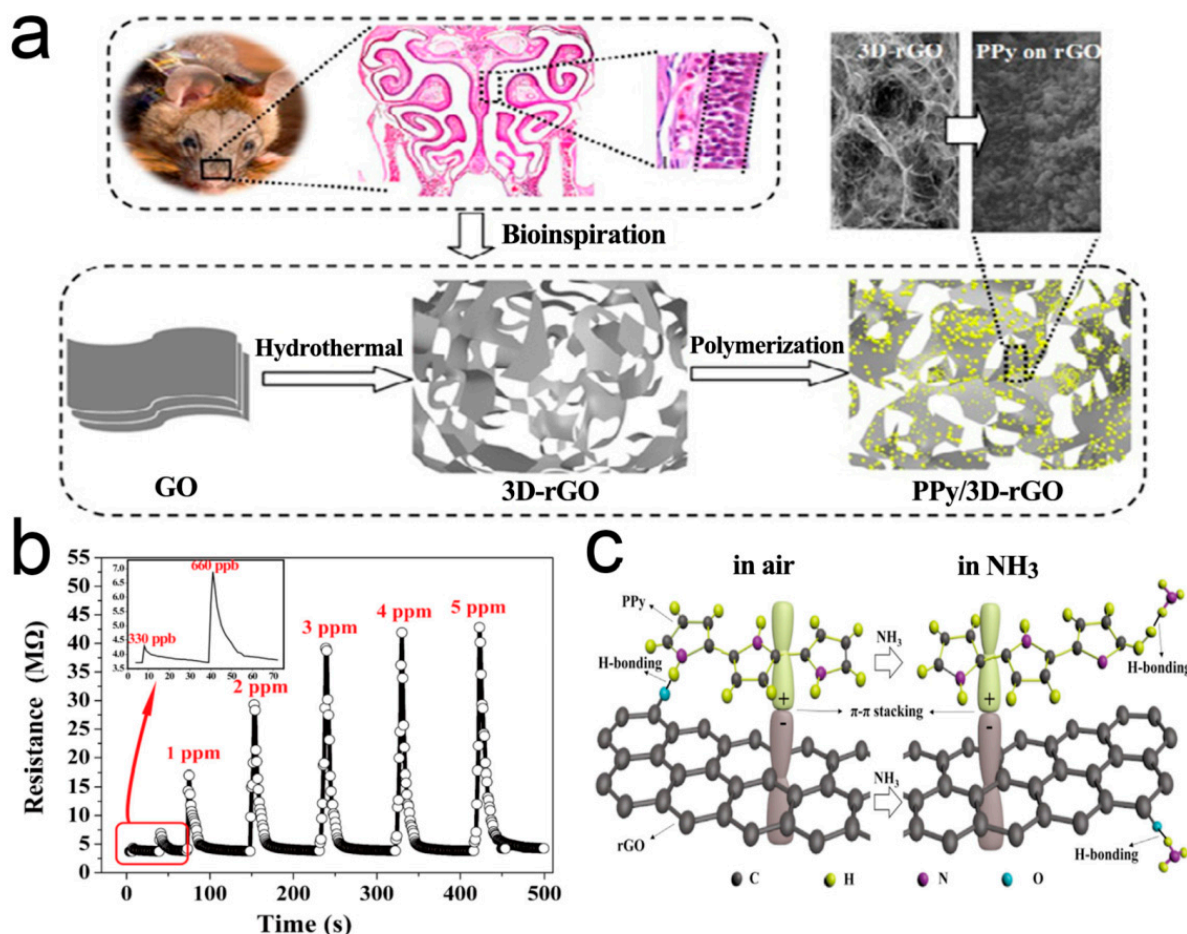


**Figure 8.** (a) Fabrication process for the 3D crumpled PPy/3D-rGO nanocomposite; (b) Dynamic response of the PPy/3D-rGO sensor to NH<sub>3</sub>; (c) Schematic illustration depicting the interaction of NH<sub>3</sub> with PPy/3D-RGO [129].

#### 4.3. PANI/CuO@3D-NGF

CuO nanoparticles are suitable for the gas detection due to their narrow band gap and adjustable morphology [130–132]. However, the problem is that they can only operate effectively at high temperatures. To improve this problem, nanoparticles can be incorporated into porous materials to construct the functional composites [102,133]. Tabar et al. [134] prepared a chemical-resistant ammonia sensor based on polyaniline (PANI)/CuO nanoparticles, supported on a 3D N-doped graphene framework (NGF). The sensor has an excellent response to 100 ppm NH<sub>3</sub>, with an outstanding LOD down to 50 ppb. The average response time is 30 s at room temperature. It is not sensitive to other gases and has good selectivity to NH<sub>3</sub>. The excellent sensing performance was attributed to 3D interconnected porous structure, remarkable enhancement of charge carriers, and modified π-interactions between molecules [134].

#### 5. Phenol Gas Sensors

Phenol is the natural component of many substances and can be emitted from the combustion of fossil fuels and tobacco [20]. It is also present in animal wastes and decomposing organic material. More importantly, it is a chemical product produced at a rate of about 6 million ton/year worldwide [20]. The manufacture and transportation of phenol as well as its many uses may lead to worker exposures to this substance with health risks [135]. In 2013, Liu et al. [136] prepared an electrochemical sensor using assembled 3D graphene as the electrode. The LOD of the phenol sensor mediated by tyrosine was successfully achieved down to 50 ppm. In 2016, Guo et al. [137] reported RGO/metal-oxide *p-n* heterojunction aerogels as efficient 3D sensing frameworks for phenol detection. Upon

the detection of phenol at room temperature, the sensor has good sensitivity, repeatability, and stability. The linear relationship is in the range of 10–80 ppb. Compared with the detection results of ethanol, toluene, and methanol, the gas sensor based on RGO/SnO<sub>2</sub> composite aerogel has much higher sensitivity to phenol with the LOD down to 5 ppb. In the same year, Gao et al. [138] reported highly sensitive electrocatalytic determination of phenols based on coupled cMWCNT/cyclodextrin edge-functionalized graphene composite. The sensor has excellent performance towards trace detection of three typical phenols (4-aminophenol, 4-AP; 4-chlorophenol, 4-CP; 4-nitrophenol, 4-NP). Under optimal conditions, the current responses of 4-AP, 4-CP, and 4-NP are linear to concentrations over two different ranges, with the LODs of 0.019, 0.017, and 0.027 ppm ( $S/N = 3$ ), respectively. In 2019, Qi et al. [139] reported a facile synthesis of 3D S/N co-doped graphene derived from GO hydrogel. This newly fabricated sensor was used in the simultaneous detection of catechol and hydroquinone, with the LODs of 0.28 and 0.15 ppm, respectively.

## 6. Conclusions

Compared with the 2D graphene nanosheets, the signal transduction of 3D graphene frameworks are more than ten times higher in most gas detection, due to the increase of the interaction surface area and the number of active adsorption sites [89]. In addition to the original 2D structural properties of graphene, its 3D porous frameworks are more favorable. It is good for adsorption and diffusion of gas molecules. In general, the LOD can be improved from ppm level to several ppb level. This has a great impact on the prevention of toxic and harmful air pollution to the atmosphere.

In addition, 3D graphene has a strong mechanical strength and a high temperature resistance, capable of using in harsh environments. These properties are very promising for practical application. It is a potential research direction to combine 3D graphene with flexible substrate to make wearable flexible sensors.

However, 3D graphene is still limited in wide applications due to its limited gas sensing types. The main toxic pollutants in the air are NO<sub>x</sub> (main NO<sub>2</sub>), NH<sub>3</sub>, CO, CH<sub>2</sub>O, and phenol. Compared with traditional metal oxide sensing materials, graphene is superior due to the much lower operating temperature and much lower resistance. It requires a low energy consumption in operation [83,87,115]. As shown in Table 2, traditional semiconductor-based gas sensors generally work at 200–400 °C [98,140–142]. Some commercial gas sensors could work well at room temperature, but with some performance loss of the LOD [143,144]. Compared to individual MoS<sub>2</sub>, SnS<sub>2</sub>, organic compounds (e.g., PPy), and semiconductor metal oxides (e.g., SnO<sub>2</sub>), the sensors based on 3D graphene composites could see an increase of the sensitivity.

At present, 3D graphene is mainly sensitive to NO<sub>2</sub> and NH<sub>3</sub>, and more gas sensors need to be discovered. The adsorption and desorption of 3D graphene need to be accelerated so as to reduce the response and recovery times of the sensor. Finally, 3D graphene sensors are still in the stage of laboratory investigation, and more work is needed to put forward these developments to the commercialization stage.

**Table 2.** Sensing performance comparison of 3D graphene and other semiconductor materials including commercial sensors.

Sensing Materials	Gas	Temp. (°C)	C <sub>gas</sub> (ppm)	Response	S (ppm <sup>-1</sup> )	Recovery Time (s)	LOD (ppb)	Year	Ref.
MoS <sub>2</sub>	NO <sub>2</sub>	80	10	ΔI/I <sub>0</sub> = 120%	12%	-	-	2019	[52]
3D MoS <sub>2</sub> /RGO	NO <sub>2</sub>	80	10	ΔI/I <sub>0</sub> = 2483%	248%	30	27.9	2019	[52]
SnS <sub>2</sub>	NO <sub>2</sub>	160	8	ΔG/G <sub>0</sub> = 28%	3.5%	140	20–30	2015	[98]
3D SnS <sub>2</sub> /RGO	NO <sub>2</sub>	RT	8	ΔG/G <sub>0</sub> = 49.8%	6.1%	76	8.7	2020	[86]
SnO <sub>2</sub>	NO <sub>2</sub>	400	5	ΔR/R <sub>0</sub> = 10%	2%	720	-	2016	[142]
3D SnO <sub>2</sub> /RGOH	NO <sub>2</sub>	RT	5	ΔG/G <sub>0</sub> = 32%	4.3%	260	2.8	2020	[85]
PPy	NH <sub>3</sub>	RT	3	R <sub>g</sub> /R <sub>a</sub> = 2%	0.6%	-	-	2019	[129]
3D RGO/PPy	NH <sub>3</sub>	RT	3	R <sub>g</sub> /R <sub>a</sub> = 10.5%	10.5%	25	-	2019	[129]
TypeNO <sub>2</sub> /S-100	NO <sub>2</sub>	RT	1	$-370 \pm 70 (\text{nA} \cdot \text{ppm}^{-1})$		<60	<200	Comm.	[143]
TypeNH <sub>3</sub> /SR-200	NH <sub>3</sub>	RT	1	$90 \pm 18 (\text{nA} \cdot \text{ppm}^{-1})$		<50	<600	Comm.	[144]

**Author Contributions:** Conceptualization, Q.D., M.X. and Z.C.; methodology, M.X.; software, Q.D.; validation, G.L., Y.Z. and Z.C.; formal analysis, Q.D.; investigation, Z.C.; resources, M.X.; data curation, Q.D.; writing—original draft preparation, Q.D. and M.X.; writing—review and editing, Z.C.; visualization, Q.D.; supervision, Y.Z. and Z.C.; project administration, Z.C.; funding acquisition, Z.C. All authors have read and agreed to the published version of the manuscript.

**Funding:** This research received no external funding.

**Institutional Review Board Statement:** Not applicable.

**Informed Consent Statement:** Not applicable.

**Conflicts of Interest:** The authors declare no conflict of interest.

## References

- Koolen, C.D.; Rothenberg, G. Air pollution in Europe. *ChemSusChem* **2018**, *12*, 164–172. [[CrossRef](#)]
- Tong, S. Air pollution and disease burden. *Lancet Planet. Health* **2019**, *3*, 49–50. [[CrossRef](#)]
- Ranscombe, P. Wearable technology for air pollution. *Lancet Respir. Med.* **2019**, *7*, 567–568. [[CrossRef](#)]
- Liu, J. Mapping high resolution national daily NO<sub>2</sub> exposure across mainland China using an ensemble algorithm. *Environ. Pollut.* **2021**, *279*, 116932. [[CrossRef](#)] [[PubMed](#)]
- Sinharoy, S.S.; Clasen, T.; Martorell, R. Air pollution and stunting: A missing link? *Lancet Glob. Health* **2020**, *8*, 472–475. [[CrossRef](#)]
- Chen, C.; Li, W.; Dong, L.; Li, X. The effect of meteorological factors, seasonal factors and air pollutions on the formation of particulate matter. *IOP Conf. Ser. Earth Environ. Sci.* **2020**, *450*, 0120121. [[CrossRef](#)]
- Siregar, A.M.; Siregar, C.A.; Yani, M. Engineering of motorcycle exhaust gases to reduce air pollution. *IOP Conf. Ser. Mater. Sci. Eng.* **2020**, *821*, 012048. [[CrossRef](#)]
- U. S. Environmental Protection Agency. Review of the Primary National Ambient Air Quality Standards for Nitrogen Dioxide. 2015. Available online: <https://www.epa.gov/sites/production/files/2020-07/documents/20150504reaplanning.pdf> (accessed on 4 May 2021).
- Zhang, Y.; Xu, W.; Wen, Z.; Wang, D.; Hao, T.; Tang, A.; Liu, X. Atmospheric deposition of inorganic nitrogen in a semi-arid grassland of Inner Mongolia, China. *J. Arid Land* **2017**, *9*, 810–822. [[CrossRef](#)]
- Widiana, D.R.; Wang, Y.F.; You, S.J.; Yang, H.H.; Wang, L.C.; Tsai, J.H.; Chen, H.M. Air pollution profiles and health risk assessment of ambient volatile organic compounds above a municipal wastewater treatment plant, Taiwan. *Aerosol. Air Qual. Res.* **2019**, *19*, 375–382. [[CrossRef](#)]
- Naseem, S.; King, A.J. Ammonia production in poultry houses can affect health of humans, birds, and the environment—techniques for its reduction during poultry production. *Environ. Sci. Pollut. Res.* **2018**, *25*, 15269–15293. [[CrossRef](#)]
- Börü, Ü.T.; Böyük, C.; Taşemir, M.; Gezer, T.; Serim, V.A. Air pollution, a possible risk factor for multiple sclerosis. *Acta Neurol. Scand.* **2020**, *141*, 431–437. [[CrossRef](#)] [[PubMed](#)]
- National Research Council. *Acute Exposure Guideline Levels for Selected Airborne Chemicals: Volume 6*; The National Academies Press: Washington, DC, USA, 2003. Available online: <https://www.ncbi.nlm.nih.gov/books/NBK207883/> (accessed on 4 May 2021).
- Jia, C.; Cao, K.; Valaulikar, R.; Fu, X.; Sorin, A.B. Variability of total volatile organic compounds (TVOC) in the indoor air of retail stores. *Int. J. Environ. Res. Public Health* **2019**, *16*, 4622. [[CrossRef](#)] [[PubMed](#)]
- Spinelle, L.; Gerboles, M.; Kok, G.; Persijn, S.; Sauerwald, T. Review of portable and low-cost sensors for the ambient air monitoring of benzene and other volatile organic compounds. *Sensors* **2017**, *17*, 1520. [[CrossRef](#)]
- Bocos-Bintintan, V.; Ratiu, I.A. Hunting for toxic industrial chemicals: Real-time detection of carbon disulfide traces by means of ion mobility spectrometry. *Toxics* **2020**, *8*, 121. [[CrossRef](#)] [[PubMed](#)]
- Bocos-Bintintan, V.; Ghira, G.B.; Anton, M.; Martinic, A.-V.; Ratiu, I.A. Sensing precursors of illegal drugs—Rapid detection of acetic anhydride vapors at trace levels using photoionization detection and ion mobility spectrometry. *Molecules* **2020**, *61*, 1852. [[CrossRef](#)]
- Ghira, G.B.; Ratiu, I.A.; Bocos-Bintintan, V. Fast characterization of pyridine using ion mobility spectrometry and photoionization detection. *Environ. Eng. Manag. J.* **2013**, *12*, 251–256. [[CrossRef](#)]
- Patel, B.R.; Noroozifar, M.; Kerman, K. Review-Nanocomposite-based sensors for voltammetric detection of hazardous phenolic pollutants in water. *J. Electrochem. Soc.* **2020**, *167*, 037568. [[CrossRef](#)]
- Busca, G.; Berardinelli, S.; Resini, C.; Arrighi, L. Technologies for the removal of phenol from fluid streams: A short review of recent developments. *J. Hazard. Mater.* **2008**, *160*, 265–288. [[CrossRef](#)]
- Wolkoff, P.; Wilkins, C.K.; Clausen, P.A.; Nielsen, G.D. Organic compounds in office environments—Sensory irritation, odor, measurements and the role of reactive chemistry. *Indoor Air* **2006**, *16*, 7–19. [[CrossRef](#)]
- Zong, P.A.; Liang, J.; Zhang, P.; Wan, C.; Wang, Y.; Koumoto, K. Graphene-based thermoelectrics. *ACS Appl. Energy Mater.* **2020**, *3*, 2224–2239. [[CrossRef](#)]
- Varghese, S.S.; Lonkar, S.; Singh, K.K.; Swaminathan, S.; Abdala, A. Recent advances in graphene based gas sensors. *Sens. Actuator B Chem.* **2015**, *218*, 160–183. [[CrossRef](#)]

24. Cui, Y.; Liu, Q.; He, Z.; Gao, X.; Wu, E.; Guo, G.; Zhou, C.; Feng, Z. Epitaxial graphene gas sensors on SiC substrate with high sensitivity. *J. Semicond.* **2020**, *41*, 032101. [[CrossRef](#)]
25. Yoon, H.J.; Jun, D.H.; Yang, J.H.; Zhou, Z.X.; Yang, S.S.; Cheng, M.M.C. Carbon dioxide gas sensor using a graphene sheet. *Sens. Actuator B Chem.* **2011**, *157*, 310–313. [[CrossRef](#)]
26. Chung, M.G.; Kim, D.H.; Lee, H.M.; Kim, T.; Choi, J.H.; Seo, D.K.; Yoo, J.B.; Hong, S.H.; Kang, T.J.; Kim, Y.H. Highly sensitive NO<sub>2</sub> gas sensor based on ozone treated graphene. *Sens. Actuator B Chem.* **2012**, *166–167*, 172–176. [[CrossRef](#)]
27. Zhou, L.; Shen, F.; Tian, X.; Wang, D.; Zhang, T.; Chen, W. Stable Cu<sub>2</sub>O nanocrystals grown on functionalized graphene sheets and room temperature H<sub>2</sub>S gas sensing with ultrahigh sensitivity. *Nanoscale* **2013**, *5*, 1564–1569. [[CrossRef](#)]
28. Bian, S.; Shen, C.; Qian, Y.; Liu, J.; Xi, F.; Dong, X. Facile synthesis of sulfur-doped graphene quantum dots as fluorescent sensing probes for Ag<sup>+</sup> ions detection. *Sens. Actuator B Chem.* **2017**, *242*, 231–237. [[CrossRef](#)]
29. Li, X.; Li, X.; Li, Z.; Wang, J.; Zhang, J. WS<sub>2</sub> nanoflakes based selective ammonia sensors at room temperature. *Sens. Actuator B Chem.* **2017**, *240*, 273–277. [[CrossRef](#)]
30. Karmakar, N.S.; Fernandes, R.P.; Jain, S.; Patil, U.V.; Shimpi, N.G.; Bhat, N.V.; Kothari, D.C. Room temperature NO<sub>2</sub> gas sensing properties of p-toluenesulfonic acid doped silver-polypyrrole nanocomposite. *Sens. Actuator B Chem.* **2017**, *242*, 118–126. [[CrossRef](#)]
31. Zou, J.; Liu, Z.; Guo, Y.; Dong, C. Electrochemical sensor for the facile detection of trace amounts of bisphenol A based on cyclodextrin-functionalized graphene/platinum nanoparticles. *Anal. Methods* **2016**, *9*, 134–140. [[CrossRef](#)]
32. Wu, W.; Liu, Z.; Jauregui, L.A.; Yu, Q.; Pillai, R.; Cao, H.; Bao, J.; Chen, Y.P.; Pei, S.S. Wafer-scale synthesis of graphene by chemical vapor deposition and its application in hydrogen sensing. *Sens. Actuator B Chem.* **2010**, *150*, 296–300. [[CrossRef](#)]
33. Pak, Y.; Kim, S.M.; Jeong, H.; Kang, C.G.; Park, J.S.; Song, H.; Lee, R.; Myoung, N.S.; Lee, B.H.; Seo, S.; et al. Palladium-decorated hydrogen-gas sensors using periodically aligned graphene nanoribbons. *ACS Appl. Mater. Interfaces* **2014**, *6*, 13293–13298. [[CrossRef](#)]
34. Ritikos, R.; Whitcher, T.J.; Razib, N.M.; Bien, D.C.S.; Chanlek, N.; Nakajima, H.; Saisopa, T.; Songsiriritthigul, P.; Huang, N.M.; Rahman, S.A. A practical carbon dioxide gas sensor using room-temperature hydrogen plasma reduced graphene oxide. *Sens. Actuator B Chem.* **2014**, *193*, 692–700. [[CrossRef](#)]
35. Yasaei, P.; Kumar, B.; Hantehzadeh, R.; Kayyalha, M.; Baskin, A.; Repnin, N.; Wang, C.H.; Klie, F.R.; Chen, Y.P.; Král, P.; et al. Chemical sensing with switchable transport channels in graphene grain boundaries. *Nat. Commun.* **2014**, *5*, 4911. [[CrossRef](#)]
36. Wu, Z.; Chen, X.; Zhu, S.; Zhou, Z.; Yao, Y.; Quan, W.; Liu, B. Enhanced sensitivity of ammonia sensor using graphene/polyaniline nanocomposite. *Sens. Actuator B Chem.* **2013**, *178*, 485–493. [[CrossRef](#)]
37. Johnson, J.L.; Behnam, A.; Pearton, S.J.; Ural, A. Hydrogen sensing using Pd-functionalized multi-layer graphene nanoribbon networks. *Adv. Mater.* **2010**, *22*, 4877–4880. [[CrossRef](#)]
38. Kumar, R.; Avasthi, D.K.; Kaur, A. Fabrication of chemiresistive gas sensors based on multistep reduced graphene oxide for low parts per million monitoring of sulfur dioxide at room temperature. *Sens. Actuator B Chem.* **2017**, *242*, 461–468. [[CrossRef](#)]
39. Akhter, F.; Alahi, M.E.E.; Siddiquei, H.R.; Gooneratne, C.P.; Mukhopadhyay, S.C. Graphene oxide (GO) coated impedimetric gas sensor for selective detection of carbon dioxide (CO<sub>2</sub>) with temperature and humidity compensation. *IEEE Sens. J.* **2021**, *21*, 4241–4249. [[CrossRef](#)]
40. Ratinac, K.R.; Yang, W.; Ringer, S.P.; Braet, F. Toward ubiquitous environmental gas sensors—Capitalizing on the promise of graphene. *Environ. Sci. Technol.* **2010**, *44*, 1167–1176. [[CrossRef](#)] [[PubMed](#)]
41. Ali, S.; Hassan, A.; Hassan, G.; Bae, J.; Lee, C.H. All-printed humidity sensor based on gmethyl-red/methyl-red composite with high sensitivity. *Carbon* **2016**, *105*, 23–32. [[CrossRef](#)]
42. Jang, J.; Han, J.I. High performance cylindrical capacitor as a relative humidity sensor for wearable computing device. *J. Electrochem. Soc.* **2017**, *164*, B136–B141. [[CrossRef](#)]
43. Chung, M.G.; Kim, D.H.; Seo, D.K.; Kim, T.; Im, H.U.; Lee, H.M.; Yoo, J.B.; Hong, S.H.; Kang, T.J.; Kim, Y.H. Flexible hydrogen sensors using graphene with palladium nanoparticle decoration. *Sens. Actuator B Chem.* **2012**, *169*, 387–392. [[CrossRef](#)]
44. Cuong, T.V.; Pham, V.H.; Chung, J.S.; Shin, E.W.; Yoo, D.H.; Hahn, S.H.; Huh, J.S.; Rue, G.H.; Kim, E.J.; Hur, S.H.; et al. Solution-processed ZnO-chemically converted graphene gas sensor. *Mater. Lett.* **2010**, *64*, 2479–2482. [[CrossRef](#)]
45. Choi, S.J.; Choi, C.; Kim, S.J.; Cho, H.J.; Hakim, M.; Jeon, S.; Kim, I.D. Highly efficient electronic sensitization of non-oxidized graphene flakes on controlled pore-loaded WO<sub>3</sub> nanofibers for selective detection of H<sub>2</sub>S molecules. *Sci. Rep.* **2015**, *5*, 8067. [[CrossRef](#)] [[PubMed](#)]
46. Gautam, M.; Jayatissa, A.H. Ammonia gas sensing behavior of graphene surface decorated with gold nanoparticles. *Solid State Electron.* **2012**, *78*, 159–165. [[CrossRef](#)]
47. Jiang, L.; Fan, Z. Design of advanced porous graphene materials: From graphene nanomesh to 3D architectures. *Nanoscale* **2014**, *6*, 1922–1945. [[CrossRef](#)] [[PubMed](#)]
48. Duy, L.T.; Kim, D.J.; Trung, T.Q.; Dang, V.Q.; Kim, B.Y.; Moon, H.K.; Lee, N.E. High performance three-dimensional chemical sensor platform using reduced graphene oxide formed on high aspect-ratio micropillars. *Adv. Funct. Mater.* **2015**, *25*, 883–890. [[CrossRef](#)]
49. Meng, F.-L.; Guo, Z.; Huang, X.-J. Graphene-based hybrids for chemiresistive gas sensors. *Trends Anal. Chem.* **2015**, *68*, 37–47. [[CrossRef](#)]

50. Xia, Y.; Li, R.; Chen, R.; Wang, J.; Xiang, L. 3D Architectured graphene/metal oxide hybrids for gas sensors: A review. *Sensors* **2018**, *18*, 1456. [[CrossRef](#)]
51. Ilnicka, A.; Lukaszewicz, J.P. Graphene-based hydrogen gas sensors: A review. *Processes* **2020**, *8*, 633. [[CrossRef](#)]
52. Chen, T.; Yan, W.; Xu, J.; Li, J.; Zhang, G.; Ho, D. Highly sensitive and selective NO<sub>2</sub> sensor based on 3D MoS<sub>2</sub>/rGO composites prepared by a low temperature self-assembly method. *J. Alloys Compd.* **2019**, *793*, 541–551. [[CrossRef](#)]
53. Xu, Y.; Sheng, K.; Li, C.; Shi, G. Self-Assembled graphene hydrogel via a one-step hydrothermal process. *ACS Nano* **2010**, *4*, 4324–4330. [[CrossRef](#)]
54. Yin, S.; Niu, Z.; Chen, X. Assembly of graphene sheets into 3D macroscopic structures. *Small* **2012**, *8*, 2458–2463. [[CrossRef](#)]
55. Li, C.; Shi, G. Functional gels based on chemically modified graphenes. *Adv. Mater.* **2014**, *26*, 3992–4012. [[CrossRef](#)]
56. Chen, J.; Sheng, K.; Luo, P.; Li, C.; Shi, G. Graphene hydrogels deposited in nickel foams for high-rate electrochemical capacitors. *Adv. Mater.* **2012**, *24*, 4569–4573. [[CrossRef](#)]
57. Li, C.; Shi, G. Three-dimensional graphene architectures. *Nanoscale* **2012**, *4*, 5549–5563. [[CrossRef](#)]
58. Sui, Z.; Zhang, X.; Lei, Y.; Luo, Y. Easy and green synthesis of reduced graphite oxide-based hydrogels. *Carbon* **2011**, *49*, 4314–4321. [[CrossRef](#)]
59. Zhang, X.; Sui, Z.; Xu, B.; Yue, S.; Luo, Y.; Zhan, W.; Liu, B. Mechanically strong and highly conductive graphene aerogel and its use as electrodes for electrochemical power sources. *J. Mater. Chem.* **2011**, *21*, 6494–6497. [[CrossRef](#)]
60. Wu, Q.; Sun, Y.; Bai, H.; Shi, G. High-performance supercapacitor electrodes based on graphene hydrogels modified with 2-aminoanthraquinone moieties. *Phys. Chem. Chem. Phys.* **2011**, *13*, 11193–11198. [[CrossRef](#)]
61. Chen, W.; Li, S.; Chen, C.; Yan, L. Self-assembly and embedding of nanoparticles by in situ reduced graphene for preparation of a 3D graphene/nanoparticle aerogel. *Adv. Mater.* **2011**, *23*, 5679–5683. [[CrossRef](#)]
62. Pham, H.D.; Pham, V.H.; Cuong, T.V.; Nguyen-Phan, T.D.; Chung, J.S.; Shin, E.W.; Kim, S. Synthesis of the chemically converted graphene xerogel with superior electrical conductivity. *Chem. Commun.* **2011**, *47*, 9672–9674. [[CrossRef](#)] [[PubMed](#)]
63. Chen, M.; Zhang, C.; Li, X.; Zhang, L.; Ma, Y.; Zhang, L.; Xu, X.; Xia, F.; Wang, W.; Gao, J. A one-step method for reduction and self-assembling of graphene oxide into reduced graphene oxide aerogels. *J. Mater. Chem. A* **2013**, *1*, 2869–2877. [[CrossRef](#)]
64. Luan, V.H.; Tien, H.N.; Le, T.H.; Hien, N.T.M.; Hur, S.H. Synthesis of a highly conductive and large surface area graphene oxide hydrogel and its use in a supercapacitor. *J. Mater. Chem. A* **2012**, *1*, 208–211. [[CrossRef](#)]
65. Sheng, K.X.; Xu, Y.X.; Li, C.; Shi, Q.G. High-performance self-assembled graphene hydrogels prepared by chemical reduction of graphene oxide. *New Carbon Mater.* **2011**, *26*, 9–15. [[CrossRef](#)]
66. Chen, K.; Chen, L.; Chen, Y.; Bai, H.; Li, L. Three-dimensional porous graphene-based composite materials: Electrochemical synthesis and application. *J. Mater. Chem.* **2012**, *22*, 20968–20976. [[CrossRef](#)]
67. Shadkam, R.; Naderi, M.; Ghazitabar, A.; Asghari-Alamdar, A.; Shateri, S. Enhanced electrochemical performance of graphene aerogels by using combined reducing agents based on mild chemical reduction method. *Ceram. Int.* **2020**, *46*, 22197–22207. [[CrossRef](#)]
68. Li, Y.; Sheng, K.; Yuan, W.; Shi, G. A high-performance flexible fibre-shaped electrochemical capacitor based on electrochemically reduced graphene oxide. *Chem. Commun.* **2012**, *49*, 291–293. [[CrossRef](#)] [[PubMed](#)]
69. Yang, X.; Qiu, L.; Cheng, C.; Wu, Y.; Ma, Z.F.; Li, D. Ordered gelation of chemically converted graphene for next-generation electroconductive hydrogel films. *Angew. Chem. Int. Ed.* **2011**, *50*, 7325–7328. [[CrossRef](#)]
70. Yang, X.; Zhu, J.; Qiu, L.; Li, D. Bioinspired effective prevention of restacking in multilayered graphene films: Towards the next generation of high-performance supercapacitors. *Adv. Mater.* **2011**, *23*, 2833–2838. [[CrossRef](#)]
71. Sun, Y.; Wu, Q.; Shi, G. Supercapacitors based on self-assembled graphene organogel. *Phys. Chem. Chem. Phys.* **2011**, *13*, 17249–17254. [[CrossRef](#)]
72. Zhou, Q.; Gao, J.; Li, C.; Chen, J.; Shi, G. Composite organogels of graphene and activated carbon for electrochemical capacitors. *J. Mater. Chem. A* **2013**, *1*, 9196–9201. [[CrossRef](#)]
73. Gun, J.; Kulkarni, S.A.; Xiu, W.; Batabyal, S.K.; Sladkevich, S.; Prikhodchenko, P.V.; Gutkin, V.; Lev, O. Graphene oxide organogel electrolyte for quasi solid dye sensitized solar cells. *Electrochim. Commun.* **2012**, *19*, 108–110. [[CrossRef](#)]
74. Nardecchia, S.; Carriazo, D.; Ferrer, M.L.; Gutiérrez, M.C.; Monte, F.D. Three dimensional macroporous architectures and aerogels built of carbon nanotubes and/or graphene: Synthesis and applications. *Chem. Soc. Rev.* **2013**, *42*, 794–830. [[CrossRef](#)]
75. Hu, H.; Zhao, Z.; Wu, W.; Gogotsi, Y.; Qiu, J. Ultralight and highly compressible graphene aerogels. *Adv. Mater.* **2012**, *25*, 2219–2223. [[CrossRef](#)] [[PubMed](#)]
76. Li, W.L.; Lu, K.; Walz, J.Y. Freeze casting of porous materials: Review of critical factors in microstructure evolution. *Int. Mater. Rev.* **2012**, *57*, 37–60. [[CrossRef](#)]
77. Qiu, L.; Liu, J.Z.; Chang, S.L.Y.; Wu, Y.; Li, D. Biomimetic superelastic graphene-based cellular monoliths. *Nat. Commun.* **2012**, *3*, 1241. [[CrossRef](#)] [[PubMed](#)]
78. Donarelli, M.; Prezioso, S.; Perrozzi, F.; Bisti, F.; Nardone, M.; Giancaterini, L.; Ottaviano, L.; Cantalini, C. Response to NO<sub>2</sub> and other gases of resistive chemically exfoliated MoS<sub>2</sub>-based gas sensors. *Sens. Actuator B Chem.* **2015**, *207*, 602–613. [[CrossRef](#)]
79. Ratiu, I.A.; Ligor, T.; Bocos-Bintintan, V.; Mayhew, C.A.; Buszewski, B. Volatile organic compounds in exhaled breath as fingerprints of lung cancer, asthma and COPD. *J. Clin. Med.* **2020**, *10*, 32. [[CrossRef](#)]
80. Wu, J.; Tao, K.; Miao, J.; Norford, L.K. Improved selectivity and sensitivity of gas sensing using a 3D reduced graphene oxide hydrogel with an integrated microheater. *ACS Appl. Mater. Interfaces* **2015**, *7*, 27502–27510. [[CrossRef](#)] [[PubMed](#)]

81. Yuan, W.; Huang, L.; Zhou, Q.; Shi, G. Ultrasensitive and selective nitrogen dioxide sensor based on self-assembled graphene/polymer composite nanofibers. *ACS Appl. Mater. Interfaces* **2014**, *6*, 17003–17008. [[CrossRef](#)]
82. Wu, J.; Li, Z.; Xie, X.; Tao, K.; Liu, C.; Khor, K.A.; Miao, J.; Norford, L.K. 3D superhydrophobic reduced graphene oxide for activated NO<sub>2</sub> sensing with enhanced immunity to humidity. *J. Mater. Chem. A* **2018**, *6*, 478–488. [[CrossRef](#)]
83. Wu, J.; Tao, K.; Guo, Y.; Li, Z.; Wang, X.; Luo, Z.; Feng, S.; Du, C.; Chen, D.; Miao, J.; et al. A 3D chemically modified graphene hydrogel for fast, highly sensitive, and selective gas sensor. *Adv. Sci.* **2017**, *4*, 1600319. [[CrossRef](#)] [[PubMed](#)]
84. Li, L.; He, S.; Liu, M.; Zhang, C.; Chen, W. Three-dimensional mesoporous graphene aerogel-supported SnO<sub>2</sub> nanocrystals for high-performance NO<sub>2</sub> gas sensing at low temperature. *Anal. Chem.* **2015**, *87*, 1638–1645. [[CrossRef](#)] [[PubMed](#)]
85. Wu, J.; Wu, Z.; Ding, H.; Wei, Y.; Huang, W.; Yang, X.; Li, Z.; Qiu, L.; Wang, X. Three-dimensional graphene hydrogel decorated with SnO<sub>2</sub> for high-performance NO<sub>2</sub> sensing with enhanced immunity to humidity. *ACS Appl. Mater. Interfaces* **2020**, *12*, 2634–2643. [[CrossRef](#)]
86. Wu, J.; Wu, Z.; Ding, H.; Wei, Y.; Huang, W.; Yang, X.; Li, Z.; Qiu, L.; Wang, X. Flexible, 3D SnS<sub>2</sub>/reduced graphene oxide heterostructured NO<sub>2</sub> sensor. *Sens. Actuator B Chem.* **2020**, *305*, 127445. [[CrossRef](#)]
87. Wu, J.; Wu, Z.; Ding, H.; Yang, X.; Wei, Y.; Xiao, M.; Yang, Z.; Yang, B.-R.; Liu, C.; Lu, X.; et al. Three-dimensional-structured boron- and nitrogen-doped graphene hydrogel enabling high-sensitivity NO<sub>2</sub> detection at room temperature. *ACS Sens.* **2019**, *4*, 1889–1898. [[CrossRef](#)]
88. Zhu, P.; Li, S.; Zhao, C.; Zhang, Y.; Yu, J. 3D synergistical rGO/Eu(TPyP)(Pc) hybrid aerogel for high-performance NO<sub>2</sub> gas sensor with enhanced immunity to humidity. *J. Hazard. Mater.* **2019**, *384*, 121426. [[CrossRef](#)]
89. Wu, J.; Wei, Y.; Ding, H.; Wu, Z.; Yang, X.; Li, Z.; Huang, W.; Xie, X.; Tao, K.; Wang, X. Green synthesis of 3D chemically functionalized graphene hydrogel for high-performance NH<sub>3</sub> and NO<sub>2</sub> detection at room temperature. *ACS Appl. Mater. Interfaces* **2020**, *12*, 20623–20632. [[CrossRef](#)]
90. Kumar, R.; Goel, N.; Kumar, M. UV-activated MoS<sub>2</sub> based fast and reversible NO<sub>2</sub> sensor at room temperature. *ACS Sens.* **2017**, *2*, 1744–1752. [[CrossRef](#)]
91. Xu, T.; Pei, Y.; Liu, Y.; Wu, D.; Shi, Z.; Xu, J.; Tian, Y.; Li, X. High-response NO<sub>2</sub> resistive gas sensor based on bilayer MoS<sub>2</sub> grown by a new two-step chemical vapor deposition method. *J. Alloys Compd.* **2017**, *725*, 253–259. [[CrossRef](#)]
92. Zhou, Y.; Zou, C.; Lin, X.; Guo, Y. UV light activated NO<sub>2</sub> gas sensing based on Au nanoparticles decorated few-layer MoS<sub>2</sub> thin film at room temperature. *Appl. Phys. Lett.* **2018**, *113*, 082103. [[CrossRef](#)]
93. Zhou, Y.; Gao, C.; Guo, Y. UV assisted ultrasensitive trace NO<sub>2</sub> gas sensing based on few-layer MoS<sub>2</sub> nanosheet-ZnO nanowire heterojunctions at room temperature. *J. Mater. Chem. A* **2018**, *6*, 10286–10296. [[CrossRef](#)]
94. Agrawal, A.V.; Kumar, R.; Venkatesan, S.; Zakhidov, A.; Yang, G.; Bao, J.; Kumar, M.; Kumar, M. Photoactivated mixed In-plane and edge-enriched p-Type MoS<sub>2</sub> Flake-Based NO<sub>2</sub> sensor working at room temperature. *ACS Sens.* **2018**, *3*, 998–1004. [[CrossRef](#)]
95. Wang, Z.; Zhang, T.; Zhao, C.; Han, T.; Fei, T.; Liu, S.; Lu, G. Rational synthesis of molybdenum disulfide nanoparticles decorated reduced graphene oxide hybrids and their application for high-performance NO<sub>2</sub> sensing. *Sens. Actuator B Chem.* **2018**, *260*, 508–518. [[CrossRef](#)]
96. Zhou, Y.; Liu, G.; Zhu, X.; Guo, Y. Ultrasensitive NO<sub>2</sub> gas sensing based on rGO/MoS<sub>2</sub> nanocomposite film at low temperature. *Sens. Actuator B Chem.* **2017**, *251*, 280–290. [[CrossRef](#)]
97. Yun, Y.J.; Hong, W.G.; Kim, D.Y.; Kim, H.J.; Jun, Y.; Lee, H.K. E-textile gas sensors composed of molybdenum disulfide and reduced graphene oxide for high response and reliability. *Sens. Actuator B Chem.* **2017**, *248*, 829–835. [[CrossRef](#)]
98. Ou, J.Z.; Ge, W.; Carey, B.; Daeneke, T.; Rotbart, A.; Shan, W.; Wang, Y.; Fu, Z.; Chrimes, A.F.; Włodarski, W.; et al. Physisorption-based charge transfer in two-dimensional SnS<sub>2</sub> for selective and reversible NO<sub>2</sub> gas sensing. *ACS Nano* **2015**, *9*, 10313–10323. [[CrossRef](#)]
99. Huang, Y.; Jiao, W.; Chu, Z.; Ding, G.; Yang, M.; Zhong, X.; Wang, R. Ultrasensitive ppb-level NO<sub>2</sub> gas sensors at room temperature based on SnS<sub>2</sub>/rGO nanohybrids with P-N transition property and optoelectronic visible light enhancement performance. *J. Mater. Chem. C* **2019**, *7*, 8616–8625. [[CrossRef](#)]
100. Chen, H.; Chen, Y.; Zhang, H.; Zhang, D.W.; Zhou, P.; Huang, J. Suspended SnS<sub>2</sub> layers by light assistance for ultrasensitive ammonia detection at room temperature. *Adv. Funct. Mater.* **2018**, *28*, 1801035. [[CrossRef](#)]
101. Hsiao, M.C.; Liao, S.H.; Yen, M.Y.; Liu, P.I.; Pu, N.W.; Wang, C.A.; Ma, C.C.M. Preparation of covalently functionalized graphene using residual oxygen-containing functional groups. *ACS Appl. Mater. Interfaces* **2010**, *2*, 3092–3099. [[CrossRef](#)]
102. Deng, S.; Tjoa, V.; Fan, H.M.; Tan, H.R.; Sayle, D.C.; Olivo, M.; Mhaisalkar, S.; Wei, J.; Sow, C.H. Reduced graphene oxide conjugated Cu<sub>2</sub>O nanowire mesocrystals for high-performance NO<sub>2</sub> gas sensor. *J. Am. Chem. Soc.* **2012**, *134*, 4905–4917. [[CrossRef](#)] [[PubMed](#)]
103. Xiao, Y.; Yang, Q.; Wang, Z.; Zhang, R.; Gao, Y.; Sun, P.; Sun, Y.; Lu, G. Improvement of NO<sub>2</sub> gas sensing performance based on discoid tin oxide modified by reduced graphene oxide. *Sens. Actuator B Chem.* **2016**, *227*, 419–426. [[CrossRef](#)]
104. Wang, Z.; Zhang, T.; Han, T.; Fei, T.; Liu, S.; Lu, G. Oxygen vacancy engineering for enhanced sensing performances: A case of SnO<sub>2</sub> nanoparticles-reduced graphene oxide hybrids for ultrasensitive ppb-level room-temperature NO<sub>2</sub> sensing. *Sens. Actuator B Chem.* **2018**, *266*, 812–822. [[CrossRef](#)]
105. Lee, J.H.; Katoch, A.; Choi, S.W.; Kim, J.H.; Kim, H.W.; Kim, S.S. Extraordinary Improvement of Gas-sensing performances in SnO<sub>2</sub> nanofibers due to creation of local p-n heterojunctions by loading reduced graphene oxide nanosheets. *ACS Appl. Mater. Interfaces* **2015**, *7*, 3101–3109. [[CrossRef](#)]

106. Russo, P.A.; Donato, N.; Leonardi, S.G.; Baek, S.; Conte, D.E.; Neri, G.; Pinna, N. Room-temperature hydrogen sensing with heteronanostructures based on reduced graphene oxide and Tin oxide. *Angew. Chem. Int. Ed.* **2012**, *124*, 11215–11219. [[CrossRef](#)]
107. Lv, R.; Chen, G.; Li, Q.; McCreary, A.; Botello-Méndez, A.; Morozov, S.V.; Liang, L.; Declerck, X.; Perea-López, N.; Cullen, D.A.; et al. Ultrasensitive gas detection of large-area boron-doped graphene. *Proc. Nat. Acad. Sci. USA* **2015**, *112*, 14527–14532. [[CrossRef](#)] [[PubMed](#)]
108. Dai, J.; Yuan, J.; Giannozzi, P. Gas adsorption on graphene doped with B, N, Al, and S. A theoretical study. *Appl. Phys. Lett.* **2009**, *95*, 232105. [[CrossRef](#)]
109. Ma, C.; Shao, X.; Cao, D. Nitrogen-doped graphene as an excellent candidate for selective gas sensing. *Sci. China Chem.* **2014**, *57*, 911–917. [[CrossRef](#)]
110. Shaik, M.; Rao, V.K.; Gupta, M.; Murthy, K.S.R.C.; Jain, R. Chemiresistive gas sensor for the sensitive detection of nitrogen dioxide based on nitrogen doped graphene nanosheets. *RSC Adv.* **2015**, *6*, 1527–1534. [[CrossRef](#)]
111. Wang, H.; Maiyalagan, T.; Wang, X. Review on recent progress in nitrogen-doped graphene: Synthesis, characterization, and Its potential applications. *ACS Catal.* **2012**, *2*, 781–794. [[CrossRef](#)]
112. Choudhuri, I.; Patra, N.; Mahata, A.; Ahuja, R.; Pathak, B. B–N@Graphene: Highly sensitive and selective gas sensor. *J. Phys. Chem. C* **2015**, *119*, 24827–24836. [[CrossRef](#)]
113. Wei, X.L.; Chen, Y.P.; Liu, W.L.; Zhong, J.X. Enhanced gas sensor based on nitrogen-vacancy graphene nanoribbons. *Phys. Lett. A* **2012**, *376*, 559–562. [[CrossRef](#)]
114. Agnoli, S.; Favaro, M. Doping graphene with boron: A review of synthesis methods, physicochemical characterization, and emerging applications. *J. Mater. Chem. A* **2016**, *4*, 5002–5025. [[CrossRef](#)]
115. Li, H.; Xie, W.; Liu, B.; Wang, C.; Wang, Y.; Duan, X.; Li, Q.; Wang, T. Gas modulating effect in room temperature ammonia sensing. *Sens. Actuator B Chem.* **2017**, *242*, 404–411. [[CrossRef](#)]
116. Travlou, N.A.; Seredych, M.; Rodríguez-Castellón, E.; Bandosz, T.J. Insight into ammonia sensing on heterogeneous S- and N-co-doped nanoporous carbons. *Carbon* **2016**, *96*, 1014–1021. [[CrossRef](#)]
117. Singh, E.; Meyyappan, M.; Nalwa, H.S. Flexible graphene-based wearable gas and chemical sensors. *ACS Appl. Mater. Interfaces* **2017**, *9*, 34544–34586. [[CrossRef](#)]
118. Zhang, J.; Liu, X.; Neri, G.; Pinna, N. Nanostructured materials for room-temperature gas sensors. *Adv. Mater.* **2016**, *28*, 795–831. [[CrossRef](#)]
119. Gautam, M.; Jayatissa, A.H. Adsorption kinetics of ammonia sensing by graphene films decorated with platinum nanoparticles. *J. App. Phys.* **2012**, *111*, 094317. [[CrossRef](#)]
120. Yang, F.; Taggart, D.K.; Penner, R.M. Joule heating a palladium nanowire sensor for accelerated response and recovery to hydrogen gas. *Small* **2010**, *6*, 1422–1429. [[CrossRef](#)]
121. Wu, D.; Pen, Q.; Wu, S.; Wang, G.; Deng, L.; Tai, H.; Wang, L.; Yang, Y.; Dong, L.; Zhao, Y.; et al. A simple graphene NH<sub>3</sub> gas sensor via laser direct writing. *Sensors* **2018**, *18*, 4405. [[CrossRef](#)]
122. Bai, S.; Zhao, Y.; Sun, G.; Tian, Y.; Luo, R.; Li, D.; Chen, A. Ultrasensitive room temperature NH<sub>3</sub> sensor based on a graphene-polyaniline hybrid loaded on PET thin film. *Chem. Commun.* **2012**, *51*, 7524–7527. [[CrossRef](#)]
123. Basavaraja, C.; Kim, W.J.; Thinh, P.X.; Huh, D.S. Electrical conductivity studies on water-soluble polypyrrole-graphene oxide composites. *Polym. Compos.* **2011**, *32*, 2076–2083. [[CrossRef](#)]
124. Bora, C.; Dolui, S.K. Fabrication of polypyrrole/graphene oxide nanocomposites by liquid/liquid interfacial polymerization and evaluation of their optical, electrical and electrochemical properties. *Polymer* **2012**, *53*, 923–932. [[CrossRef](#)]
125. Joshi, A.; Gangal, S.A.; Gupta, S.K. Ammonia sensing properties of polypyrrole thin films at room temperature. *Sens. Actuator B Chem.* **2011**, *156*, 938–942. [[CrossRef](#)]
126. Zhao, Y.; Li, X.; Yan, B.; Li, D.; Lawes, S.; Sun, X. Significant impact of 2D graphene nanosheets on large volume change tin-based anodes in lithium-ion batteries: A review. *J. Power Sources* **2015**, *274*, 869–884. [[CrossRef](#)]
127. Chen, X.; Wong, C.K.Y.; Yuan, C.A.; Zhang, G. Nanowire-based gas sensors. *Sens. Actuator B Chem.* **2013**, *117*, 178–195. [[CrossRef](#)]
128. Sun, J.; Shu, X.; Tian, Y.; Tong, Z.; Bai, S.; Luo, R.; Li, D.; Liu, C.C. Facile preparation of polypyrrole-reduced graphene oxide hybrid for enhancing NH<sub>3</sub> sensing at room temperature. *Sens. Actuator B Chem.* **2017**, *241*, 658–664. [[CrossRef](#)]
129. Qin, Y.; Zhang, B.; Zhang, Z. Combination of PPy with three-dimensional rGO to construct bioinspired nanocomposite for NH<sub>3</sub>-sensing enhancement. *Org. Electron.* **2019**, *70*, 240–245. [[CrossRef](#)]
130. Bedi, R.K.; Singh, I. Room-temperature ammonia sensor based on cationic surfactant-assisted nanocrystalline CuO. *ACS Appl. Mater. Interfaces* **2010**, *2*, 1361–1368. [[CrossRef](#)]
131. Singh, I.; Bedi, R.K. Surfactant-assisted synthesis, characterizations, and room temperature ammonia sensing mechanism of nanocrystalline CuO. *Solid State Sci.* **2011**, *13*, 2011–2018. [[CrossRef](#)]
132. Yang, C.; Su, X.; Xiao, F.; Jian, J.; Wang, J. Gas sensing properties of CuO nanorods synthesized by a microwave-assisted hydrothermal method. *Sens. Actuator B Chem.* **2011**, *158*, 299–303. [[CrossRef](#)]
133. Hsu, Y.W.; Hsu, T.K.; Sun, C.L.; Nien, Y.T.; Pu, N.W.; Ger, M.D. Synthesis of CuO/graphene nanocomposites for nonenzymatic electrochemical glucose biosensor applications. *Electrochim. Acta* **2012**, *82*, 152–157. [[CrossRef](#)]
134. Tabar, F.A.; Nikfarjam, A.; Tavakoli, N.; Gavgani, J.N.; Mahyari, M.; Hosseini, S.G. Chemical-resistant ammonia sensor based on polyaniline/CuO nanoparticles supported on three-dimensional nitrogen-doped graphene-based framework nanocomposites. *Microchim. Acta* **2020**, *187*, 293. [[CrossRef](#)]

135. Acosta, C.A.; Pasquali, C.E.L.; Paniagua, G.; Garcinuño, R.M.; Hernando, P.F. Evaluation of total phenol pollution in water of San Martin Canal from Santiago del Estero, Argentina. *Environ. Pollut.* **2018**, *236*, 265–272. [CrossRef] [PubMed]
136. Liu, F.; Piao, Y.; Choi, J.S.; Seo, T.S. Three-dimensional graphene micropillar based electrochemical sensor for phenol detection. *Biosens. Bioelectron.* **2013**, *50*, 387–392. [CrossRef] [PubMed]
137. Guo, D.; Cai, P.; Sun, J.; He, W.; Wu, X.; Zhang, T.; Wang, X.; Zhang, X. Reduced-graphene-oxide/metal-oxide p-n heterojunction aerogels as efficient 3D sensing frameworks for phenol detection. *Carbon* **2016**, *99*, 571–578. [CrossRef]
138. Gao, J.; Liu, M.; Song, H.; Zhang, S.; Qian, Y.; Li, A. Highly-sensitive electrocatalytic determination for toxic phenols based on coupled cMWCNT/cyclodextrin edge-functionalized graphene composite. *J. Hazard. Mater.* **2016**, *318*, 99–108. [CrossRef] [PubMed]
139. Qi, Y.; Cao, Y.; Meng, X.; Cao, J.; Li, X.; Hao, Q.; Lei, W.; Li, Q.; Li, J.; Si, W. Facile synthesis of 3D sulfur/nitrogen co-doped graphene derived from graphene oxide hydrogel and the simultaneous determination of hydroquinone and catechol. *Sens. Actuator B Chem.* **2019**, *279*, 170–176. [CrossRef]
140. Hunter, G.W.; Akbar, S.; Bhansali, S.; Daniele, M.; Erb, P.D.; Johnson, K.; Liu, C.C.; Miller, D.; Oralkan, O.; Hesketh, P.J.; et al. Editors' Choice—Critical Review—A critical review of solid state gas sensors. *J. Electrochem. Chem. Soc.* **2020**, *167*, 037570. [CrossRef]
141. Dey, A. Semiconductor metal oxide gas sensors: A review. *Mater. Sci. Eng. B* **2018**, *229*, 206–217. [CrossRef]
142. Oros, C.; Horprathum, M.; Wisitsoraat, A.; Srirachayaperk, T.; Samransuksamer, B.; Limwichean, S.; Eiamchai, P.; Phokharatkul, D.; Nuntawong, N.; Chanonnonnawathorn, C.; et al. Ultra-sensitive NO<sub>2</sub> sensor based on vertically aligned SnO<sub>2</sub> nanorods deposited by DC reactive magnetron sputtering with glancing angle deposition technique. *Sens. Actuator B Chem.* **2016**, *223*, 936–945. [CrossRef]
143. Specification Sheet for Nitrogen Dioxide Gas Sensor Type NO<sub>2</sub>/S-100. Available online: <http://www.membrapor.ch/sheet/Nitrogen-Dioxide-Gas-Sensor-NO2-S-100.pdf> (accessed on 4 May 2021).
144. Specification Sheet for Ammonia Gas Sensor Type NH<sub>3</sub>/SR-200. Available online: <http://www.membrapor.ch/sheet/Ammonia-Gas-Sensor-NH3-SR-200.pdf> (accessed on 4 May 2021).